Photoinduced Dynamics of Guanosine Monophosphate in Water from Broad-Band Transient Absorption Spectroscopy and Quantum-Chemical Calculations

ARTICLE *in* JOURNAL OF THE AMERICAN CHEMICAL SOCIETY · APRIL 2009

Impact Factor: 12.11 · DOI: 10.1021/ja810092k · Source: PubMed

4 AUTHORS, INCLUDING:

Roberto Improta
Italian National Research Council
148 PUBLICATIONS **4,760** CITATIONS
SEE PROFILE

Sergey A Kovalenko
Humboldt-Universität zu Berlin
154 PUBLICATIONS **2,823** CITATIONS
SEE PROFILE

J|A|C|S ARTICLES

Published on Web 04/02/2009

Photoinduced Dynamics of Guanosine Monophosphate in Water from Broad-Band Transient Absorption Spectroscopy and Quantum-Chemical Calculations

Venugopal Karunakaran,[†] K. Kleinermanns,*[,‡] R. Improta,*[,§,||] and S. A. Kovalenko*[,†]

Department of Chemistry, Humboldt University, Brook-Taylor Street-2, D-12489 Berlin, Germany, Department of Physical Chemistry, Heinrich-Heine-University, University Street-1, D-40225 Düsseldorf, Germany, Dipartimento di Chimica, Università Federico II, Complesso Universitario Monte S. Angelo Via Cintia, I-80126 Napoli, Italy, and Istituto Biostrutture e Bioimmagini-CNR, Via Mezzocannone 16, I-80134 Napoli, Italy

Received December 30, 2008; E-mail: skovale@chemie.hu-berlin.de; kleinermanns@uni-duesseldorf.de; robimp@unina.it

Abstract: Guanosine monophosphate (GMP) in aqueous solutions has been studied with femtosecond broad-band transient absorption spectroscopy and by quantum-mechanical calculations. The sample was excited at 267 or 287 nm and probed between 270 and 1000 nm with 100 fs resolution, for various pH values between 2 and 7. At pH 2, when the guanine ring is ground-state protonated ($GMPH^+$), we observe isosbestic behavior indicating state-to-state relaxation. The relaxation is biexponential, $\tau_1 = 0.4$ ps, $\tau_2 = 2.2$ ps, and followed by slower internal conversion with $\tau_3 = 167$ ps. For nonprotonated GMP in the pH range 7−4, we find biexponential decay in the region 400−900 nm ($\tau_1 = 0.22$ ps, $\tau_2 = 0.9$ ps), whereas, between 270 and 400 nm, the behavior is triexponential with one growing, $\tau_1 = 0.25$ ps, and two decaying, $\tau_2 = 1.0$ ps, $\tau_3 = 2.5$ ps, components. The excited-state evolution is interpreted with the help of quantum-chemical calculations, performed at the time-dependent PBE0 level accounting for bulk solvent effects and specific solvation. The computed dynamics involves L_a and L_b bright excited states, whereas the $n_0\pi^*$ and $\pi\sigma^*$ dark excited states play a minor role. Independent of the pH, the photoinduced evolution involves ultrafast $L_b \rightarrow L_a$ conversion ($\tau_{ba} \ll 100$ fs) and exhibits the presence of a wide planar plateau on L_a. For neutral GMP a barrierless path connects this region to a conical intersection (CI) with the ground state, giving an account of the ultrafast decay of this species. For protonated $GMPH^+$ the system evolves into a stable minimum $L_{a\ min}$ characterized by out-of-plane displacement of NH and CH groups, which explains the longer (167 ps) fluorescence lifetime.

1. Introduction

Absorption of UV light by polynucleic acids, such as double-stranded DNA is a phenomenon of fundamental biological relevance since it can give rise to a cascade of potentially mutagenic biochemical processes (photodamage). The existence of fast and effective decay channels for the DNA excited electronic states has thus been extremely important for the development of life, decreasing the necessity of enzymatic repairs. In fact, time-resolved experiments indicate that within DNA double strands the excited-state decay occurs on a picosecond scale.[1−4] Furthermore ultrafast subpicosecond components exist which can be defined as "monomer-like," since their main features are similar to those exhibited by isolated nucleobases.[1,3] As a consequence, a full understanding of the behavior of the DNA building blocks is a prerequisite for the complete assessment of the mechanisms operative within a DNA double strand, such as the role played by intrastrand stacking interactions and interstrand hydrogen bonds. Earlier spectroscopic studies[5] established the fluorescence quantum yield of nucleobases to be $\sim 10^{-4}$ which is consistent with a short ~ 1 ps excited-state lifetime. The excited-state decay of nucleobases has since then been analyzed by a number of experimental and computational studies,[6−18] which have enabled enormous advances toward the complete assessment of the microscopic mechanisms underlying the radiationless ground-state recovery

[†] Humboldt University.
[‡] Heinrich-Heine-University.
[§] Università Federico II.
[||] Istituto Biostrutture e Bioimmagini-CNR.

(1) (a) Crespo-Hernández, C. E.; Cohen, B.; Kohler, B. *Nature (London)* **2005**, *436*, 1141. (b) Middleton, C. T.; de La Harpe, K.; Su, C.; Law, Y. K.; Crespo-Hernández, C. E.; Kohler, B. *Annu. Rev. Phys. Chem.* **2009**, *60*, 217−239.
(2) Markovitsi, D.; Talbot, F.; Gustavsson, T.; Onidas, D.; Lazzarotto, E.; Marguet, S. *Nature (London)* **2006**, *441*, E7.
(3) Schwalb, N.; Temps, F. N. *Science* **2008**, *322*, 243.
(4) Samoylova, E.; Radloff, W.; Hertel, I. V.; Sobolewski, A. L.; Domcke, W. *Science* **2004**, *306*, 1765–1768.
(5) Callis, P. R. *Annu. Rev. Phys. Chem.* **1983**, *34*, 329.
(6) Fujiwara, T.; Kamoshida, Y.; Morita, R.; Yamashita, M. *J. Photochem. Photobiol. B: Biol.* **1997**, *41*, 114.
(7) Reuther, A.; Iglev, H.; Laenen, R.; Laubereau, A *Chem. Phys. Lett.* **2000**, *325*, 368.
(8) Pecourt, J. -M. L.; Peon, J.; Kohler, B *J. Am. Chem. Soc.* **2000**, *122*, 9348.
(9) Pecourt, J. -M. L.; Peon, J.; Kohler, B. *J. Am. Chem. Soc.* **2001**, *123*, 10370.
(10) Peon, J.; Zewail, A. H. *Chem. Phys. Lett.* **2001**, *348*, 255–262.

of the lowest energy singlet states of nucleotides, nucleosides, and NA bases (thymine/uracil, cytosine, adenine, and guanine). The state-of-the-art in the field, with the focus on the ultrafast photoinduced dynamics, has recently been reviewed by Kohler and co-workers.[19]

In view of the above results it is surprising that the number of studies devoted to guanine (guanosine monophosphate, GMP) is quite limited, especially when compared to those existing for the other nucleobases. Fujiwara et al.[6] recorded the emission dynamics of GMP in aqueous solutions with a streak camera. At pH 7 they detected a 4 ps decay corresponding to neutral GMP, while at lower pH an additional slow 200 ps component was found and assigned to the protonated GMP molecule. The temporal resolution in that work was insufficient to completely resolve the ultrafast component. This difficulty was overcome by Pecourt et al.[8,9] who applied transient absorption spectroscopy with subpicosecond resolution. These authors found a 0.5 ps decay of excited-state absorption in guanosine. They assigned spectral features to the vibrationally excited hot ground state and its cooling by solute−solvent energy transfer (vibrational cooling). The subpicosecond excited-state lifetime was corroborated for GMP by Peon et al.[10] with the fluorescence upconversion technique. The fluorescence decay was measured to be monoexponential with 0.9 ps and assigned to internal conversion. However Gustavsson and co-workers[11−13] reexamined the fluorescence dynamics and found that the decays are more complex and cannot be described by a monoexponential function. For GMP they obtained a biexponential behavior with $\tau_1 = 0.2$ ps and $\tau_2 = 0.9$ ps. Recently Canuel et al.[14] studied the free nucleobases and several derivatives in the gas phase excited at 267 nm and probed via two-photon ionization at 400 nm. They reported biexponential decay with $\tau_1 = 0.15$ ps, $\tau_2 = 0.36$ ps for guanine and $\tau_1 = 0.1-0.16$ ps, $\tau_2 = 1.0-5.1$ ps for other nucleobases. The short time τ_1 was ascribed to the wave packet (WP) motion from the Franck−Condon (FC) region of the lowest excited $\pi\pi^*$ state (hereafter L_a) to its local minimum $L_{a\ \mathrm{min}}$, whereas τ_2 was rationalized by assuming that a barrier crossing is necessary to accomplish the $L_a/n\pi^*$ and $n\pi^*/S_0$ internal conversion. This interpretation has been questioned on the basis of recent computational studies. It is indeed noteworthy that many computational studies have been devoted recently to the study of guanine excited states, especially in the gas phase.[20−24]

Li et al.,[20] while agreeing that the fast τ_1 component is associated to the motion toward $L_{a\ \mathrm{min}}$, propose that the slower decay τ_2 is due to ground-state recovery through an L_a/S_0 conical intersection (CI), which is separated by a small barrier from $L_{a\ \mathrm{min}}$. Alternatively, based on minimum CASPT2/CASSCF energy reaction paths, Serrano-Andres et al.[21] propose that the τ_1 component is due to barrierless motion on L_a toward the L_a/S_0 CI, without any meaningful minimum on the L_a surface. The WP on L_a can also switch to other states, especially $n\pi^*$: this latter path, leading to an S_n/S_0 CI, is associated with the τ_2 constant. For 9H-adenine an equivalent scheme was proposed as in the case for 9H-guanine.[21] High resolution spectroscopy of 9H-adenine demonstrated vibronic coupling between the $n\pi^*$ and $\pi\pi^*$ states evidenced by the transition moment orientations in the rotational contours.[25]

The above considerations show that a definitive picture of the excited-state decay of purine nucleobases is not yet available and the underlying microscopic mechanisms cannot be considered fully assessed, especially in the condensed phase. This situation is very relevant for our understanding of the excited-state decay of double-stranded DNA since recent experiments indicate that a small number of guanine residues already lead to a significant decrease of the excited-state decay time of adenine- and thymine-based polynucleotides.[3]

One important question, which has not been experimentally addressed until now, concerns the involvement of the second bright electronic state, usually labeled as L_b, in the excited-state dynamics. GMP indeed exhibits two strong absorption bands in the near-UV (see Figure 2). A peak at 252 nm can be associated with the transition $S_0 \rightarrow L_b$, while a weaker shoulder at 280 nm is dominated by $S_0 \rightarrow L_a$. In all previous experiments the pump pulse falls at ∼267 nm, i.e., between the two bands. One may thus expect that both L_a and L_b states contribute to the experimental decays. It is also necessary to verify the role of other low-lying excited states with π/σ^* character. In the FC region $^1\pi\sigma^*$ correlates with a Rydberg state, and in the gas phase it is close in energy to L_a.[16] Its participation in the excited-state decay through abstraction of an H radical has been discarded[17] because this decay channel exhibits a significant energy barrier.[16] However it was predicted that $^1\pi\sigma^*$ exhibits a large dipole moment[16] and thus could be significantly stabilized in polar solvents.

All the questions mentioned above are tackled in the present paper which reports a comprehensive experimental and theoretical study of the photoinduced dynamics of GMP in solution. We apply broad-band transient absorption spectroscopy[26−30] which not only monitors kinetics at selected wavelengths but also gives the complete spectral evolution in a wide range, 270−1000 nm. This technique gives hints on the decay of both bright and dark states and allows discrimination of spectral shifts

(11) Gustavsson, T.; Sharonov, A.; Onidas, D.; Markovitsi, D. *Chem. Phys. Lett.* **2002**, *356*, 49.
(12) Gustavsson, T.; Sharonov, A.; Markovitsi, D. *Chem. Phys. Lett.* **2002**, *351*, 195.
(13) Onidas, D.; Markovitsi, D.; Marguet, S.; Sharonov, A.; Gustavsson, T. *J. Phys. Chem. B* **2002**, *106*, 11367–11374.
(14) Canuel, C.; Mons, M.; Piuzzi, F.; Tardivel, B.; Dimicoli, I.; Elhanine, M. *J. Chem. Phys.* **2005**, *122*, 074316.
(15) Cohen, B.; Hare, P. M.; Kohler, B. *J. Am. Chem. Soc.* **2003**, *125*, 13594.
(16) Hare, P. M.; Crespo-Hernándes, C. E.; Kohler, B. *Proc. Natl. Acad. Sci. U.S.A.* **2007**, *104*, 435.
(17) Pancur, T.; Schwalb, N. K.; Renth, F.; Temps, F. *Chem. Phys.* **2005**, *313*, 199.
(18) Schwalb, N. K.; Temps, F. *Phys. Chem. Chem. Phys.* **2006**, *8*, 5229.
(19) Crespo-Hernández, C. E.; Cohen, B.; Hare, P. M.; Kohler, B. *Chem. Rev.* **2004**, *104*, 1977–2019.
(20) Chen, H.; Li, S. H. *J. Chem. Phys.* **2006**, *124*, 154315.
(21) Serrano-Andrés, L.; Merchán, M.; Borin, A. C. *J. Am. Chem. Soc.* **2008**, *130*, 2473.
(22) (a) Yamazaki, S.; Domcke, W. *J. Phys. Chem. A* **2008**, *112*, 7090–7097. (b) Yamazaki, S.; Domcke, W.; Sobolewski, L. *J. Phys. Chem. A* **2008**, *112*, 11965–11968.
(23) Shukla, M. K.; Leszczynski, J. *J. Phys. Chem. B* **2008**, *112*, 5139–5152.
(24) Ěerný, J.; Špirko, V.; Mons, M.; Hobza, P.; Nachtigallová, D. *Phys. Chem. Chem. Phys.* **2006**, *8*, 3059–3065.
(25) Lee, Y.; Schmitt, M.; Kleinermanns, K.; Kim, B. *J. Phys. Chem.* **2006**, *110*, 11819.
(26) Kovalenko, S. A.; Dobryakov, A. L.; Ruthmann, J.; Ernsting, N. P. *Phys. Rev. A* **1999**, *59*, 2369–2381.
(27) Kovalenko, S. A.; Schanz, R.; Hennig, H.; Ernsting, N. P. *J. Chem. Phys.* **2001**, *115*, 3256–3272.
(28) Kovalenko, S. A.; Lustres, J. L. P.; Ernsting, N. P.; Rettig, W. *J. Phys. Chem. A* **2003**, *107*, 10228–10232.
(29) Pérez-Lustres, J. L.; Rodriguez-Prieto, F.; Mosquera, M.; Senyushkina, T. A.; Ernsting, N.; Kovalenko, S. A. *J. Am. Chem. Soc.* **2007**, *129*, 5408.
(30) Löwenich, D.; Kleinermanns, K.; Karunakaran, V.; Kovalenko, S. A. *Photochem. Photobiol.* **2008**, *84*, 193.

from state-to-state relaxation processes. The comparison of the results obtained with two excitation wavelengths at 267 and 287 nm provides information on the role played by the L_a and L_b states in the photoinduced evolution. Furthermore we report the dependence of transient spectra on pH in the range 2−7. As anticipated above, the excited-state dynamics of GMP at low pH is different from that in neutral solution, a result which will be analyzed in detail here.

The experimental results are interpreted with the help of quantum-chemical calculations on 9-methyl guanine (9Me-G) in solution, rooted in the density functional theory (DFT) and in its time dependent (TD) extension,[31] with the PBE0[32] functional. Solvent effects are taken into account by the polarizible continuum model (PCM),[33] while some solvent molecules from the first solvation shell are included explicitly (see Figure 1). Since guanine behaves differently in the gas phase and in solution, the inclusion of solvent effects in the theoretical treatment is important.[34,35] Here we present a study of the four lowest excited states of guanine in solution, treating both bulk solvent effects and the first solvation shell at an accurate quantum-mechanical level. It has been recognized at this point that not only bulk water may significantly modulate the excited-state decay of nucleobases, especially by affecting the relative stability of the $n\pi^*$, $\pi\pi^*$, and $\pi\sigma^*$[36−42] electronic states, but also explicit inclusion of the first solvation shell is necessary to properly model protic solvents.[31−34]

In our analysis we assume that the keto-amino tautomer of GMP dominates in water and that nonnatural guanine tautomers like the enol-amino and keto-imino forms observed in the gas phase by IR-UV spectroscopy[43−46] do not play a role in a polar solution. The analysis will thus be based on the keto-amino tautomer.

(31) (a) Dreuw, A.; Head-Gordon, M. *Chem. Rev.* **2005**, *105*, 4009. (b) Burke, K.; Werschnik, J.; Gross, E. K. U. *J. Chem. Phys.* **2005**, *123*, 62206.
(32) (a) Adamo, C.; Barone, V. *J. Chem. Phys.* **1999**, *110*, 6158–6170. (b) Ernzerhof, M.; Scuseria, G. E. *J. Chem. Phys.* **1999**, *110*, 5029–5036. (c) Adamo, C.; Scuseria, G. E.; Barone, V. *J. Chem. Phys.* **1999**, *111*, 2889–2899.
(33) Tomasi, J.; Mennucci, B.; Cammi, R. *Chem. Rev.* **2005**, *105*, 2999.
(34) Fulscher, M. P.; Serrano-Andres, L.; Roos, B. O. *J. Am. Chem. Soc.* **1997**, *119*, 6168–6176.
(35) (a) Mennucci, B.; Toniolo, A.; Tomasi, J. *J. Phys. Chem. A* **2001**, *105*, 7126–7134. (b) Shukla, M. K.; Leszczynski, J. *J. Phys. Chem. B* **2005**, *109*, 17333–1733.
(36) Perun, S.; Sobolewski, A. L.; Domcke, W. *J. Am. Chem. Soc.* **2005**, *127*, 6257.
(37) Perun, S.; Sobolewski, A. L.; Domcke, W. *J. Phys. Chem. A* **2006**, *110*, 13238.
(38) Improta, R.; Barone, V. *J. Am. Chem. Soc.* **2004**, *126*, 14320–14321.
(39) (a) Gustavsson, T.; Banyasz, A.; Lazzarotto, E.; Markovitsi, D.; Scalmani, G.; Frisch, M. J.; Barone, V.; Improta, R. *J. Am. Chem. Soc.* **2006**, *128*, 607–619. (b) Santoro, F.; Barone, V.; Gustavsson, T.; Improta, R. *J. Am. Chem. Soc.* **2006**, *128*, 16312–16322.
(40) Gustavsson, T.; Sarkar, N.; Lazzarotto, E.; Markovitsi, D.; Barone, V.; Improta, R. *J. Phys. Chem. B* **2006**, *110*, 12843–12847.
(41) Santoro, F.; Barone, V.; Improta, R. *Proc. Natl. Acad. Sci. U.S.A.* **2007**, *104*, 9931–9936.
(42) Improta, R. *Phys. Chem. Chem. Phys.* **2008**, *10*, 2656–2664.
(43) Nir, E.; Janzen, C.; Imhof, P.; Kleinermanns, K.; de Vries, M. S. *J. Chem. Phys.* **2001**, *115*, 4604.
(44) Mons, M.; Dimicoli, I.; Piuzzi, F.; Tardivel, B.; Elhanine, M. *J. Phys. Chem. A* **2002**, *106*, 5088.
(45) Seefeld, K.; Brause, R.; Häber, T.; Kleinermanns, K. *J. Phys. Chem.* **2007**, *111*, 6217.
(46) Marian, C. M. *J. Phys. Chem. A* **2007**, *111*, 1545.

Scheme 1. Guanosine 5′Monophosphate (GMP)[a]

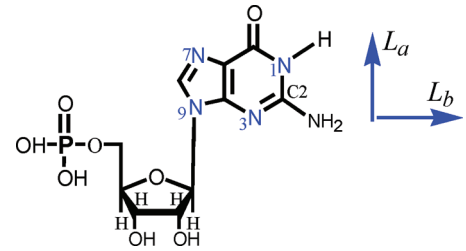

[a] The arrows indicate polarization direction of the $S_0 \rightarrow L_a$ and $S_0 \rightarrow L_b$ transitions.

2. Experimental and Computational Methods

Materials. Guanosine 5′monophosphate (Scheme 1) was received from Sigma and used without further purification. For determining the molar extinction coefficient, GMP was dried at 50 °C for 5 h under vacuum. The solution pH was adjusted with perchloric acid, and the buffer consisted of sodium chloride and 10 mM of mono sodium hydrogen phosphate.

Stationary Measurements. Absorption spectra of GMP in solution and differential absorption spectra at various temperatures were recorded with a Shimadzu UV-3101 and Varian Cary 300 spectrophotometer. Fluorescence was excited at 267 nm and measured with a Spex Fluorolog 212, and the spectra were corrected for the instrument response. All the measurements were done at ambient temperature (21 °C).

Femtosecond Measurements. The pump-supercontinuum probe technique has been described in detail elsewhere.[26−29] Two femtosecond setups are used to cover the probe range 270−1000 nm. In the first setup a Ti:Sa amplifier (Femtolasers) provides basic 30 fs pulses of 500 μJ at 800 nm with a 140 Hz repetition rate. The beam is split in two parts. 420 μJ are used to pump an optical parametric amplifier (TOPAS, Light Conversion) which delivers 50 fs, 5 μJ pump pulses at 265 nm. The remaning 80 μJ are converted into second harmonic 400 nm, 15 μJ pulses in a 0.2 mm BBO crystal. The probe supercontinuum is generated by focusing the 400 nm pulses into a 1 mm CaF_2 plate. The probe light is spectrally filtered with a dye solution flowing in a 0.3 mm cell and then split for the signal and reference. The signal beam is imaged onto the sample flow cell to a spot size of 100 μ. The sample has typically an absorbance $A = 0.7$ over a 0.3 mm thickness. The signal and reference light is dispersed with homemade grating spectrographs and finally registered by photodiode arrays with 512 pixels (S39901-512Q, Hamamatsu) covering the spectral range 270−690 nm.

With the second setup a probe region of 340−1000 nm was assessed. A regenerative Ti:Sa amplifier (CPA2001, Clark MXR) provides fundamental 150 fs pulses of 0.9 mJ at 775 nm with a 120 Hz repetition rate. The beam is split in three equal parts. The first drives a two-stage NOPA (Clark MXR) to generate 520 nm, 30 fs pulses, which in turn generate the supercontinuum probe. The second part is used to pump a single-stage NOPA from which 530 nm, 30 fs pulses are obtained. These are used after frequency doubling to pump the sample at 265 nm. The registration was similar except that the spectrographs were equipped with prisms (instead of gratings) to increase the sensitivity in the near-infrared.

Transient absorption spectra are recorded with parallel and perpendicular pump−probe polarizations and at the magic angle. The pump was blocked at every second shot to record a baseline. 50 shorts were accumulated per temporal point, and 12−18 pump−probe scans were averaged. Solute and solvent transient spectra were recorded separately and time-corrected for the chirp of the supercontinuum.[26] The pump−probe cross-correlation τ_{cc} was ∼100 fs (fwhm) across the full probe range.

Computational Methods. The absorption and emission transitions were calculated by the TDDFT method using the PBE0 exchange-correlation functional.[32] Geometry optimizations in solu-

tion were performed at the PCM/PBE0/6-31G(d) level for the ground electronic state S_0, while the excited-state geometry was optimized at the PCM/TD-PBE0/6-31G(d) level,[47] based on the linear response (LR) theory.[48] The vertical absorption ν_A and emission energies ν_E have been refined by single-point calculations employing more extended 6-31+G(d,p) and 6-311+G(2d,2p) basis sets. This approach has already been successfully applied for pyrimidine[38−40] and purine[41,42] excited states. It provides vibrationally resolved spectra in the condensed phase in agreement with experiment.[49,50]

We verified that the Kohn−Sham orbitals, mainly involved in the excitations, are similar to the Hartree−Fock ones computed with the same basis set and, thus, are suitable for quantitative interpretation. All the computed vibrational frequencies in the minima of the ground and excited states are positive. The only exception concerns 9Me-G·5H_2O, where librational modes of water can exhibit small (<50 cm^{-1}) imaginary frequencies. In each case we checked that our conclusions are not affected by small variations in the geometry of the solvation shell (see Tables S1−S3 in the Supporting Information).

Solvation Model. Bulk solvent effects on the electronic states are accounted for with the polarizable continuum model (PCM).[33] The energies ν_A and ν_E are computed with the "standard" LR implementation[47] of PCM/TD-DFT and the new state-specific (SS) one,[51,52] which allows for better treatment of the dark and bright transitions and is mandatory for a rigorous treatment of dynamical solvation effects. In brief, LR methods avoid the calculation of exact excited-state electronic densities in favor of a direct determination of excitation energies. On the other hand, in the SS procedure the excited-state electronic density and the corresponding response of surface charges (characterizing the PCM method) are self-consistently optimized with an iterative algorithm.

Our previous work[38−40,49] indicates that a satisfactory treatment of aqueous solutions requires inclusion of water molecules from the first solvation shell. Here the PCM calculations for neutral solutions (pH 7) refer to 9Me-G·5H_2O, where five water molecules are explicitly included, and to 9Me-G7H^+·6H_2O at strongly acidic conditions (pH 2, Figure 1). According to earlier studies, protonation occurs at the N7 position.[53] To verify that our results are not critically dependent on the number of H_2O molecules and to allow for conformational flexibility of the water molecule bound to N7−H, we have performed test calculations on 9Me-G7H^+·5H_2O (Figure 1). In the excited-state geometry optimizations the first solvation shell was fully optimized, i.e., was treated like solute degrees of freedom. Since outer solvation shells are not included in our calculations, this choice is expected to overestimate the conformational flexibility of the water molecules of the cybotactic region. As a consequence, the computed emission energies represent a lower bound to the experimental ones. In any case we have performed our analysis also in the absence of solvent molecules (i.e., including only the bulk solvent effect at the PCM level), to check that our results do not depend on the presence of the solvation shell (see Tables S1−S3).

When discussing solvent effects on absorption spectra we make use of two limiting cases referred to as nonequilibrium (NEQ) and

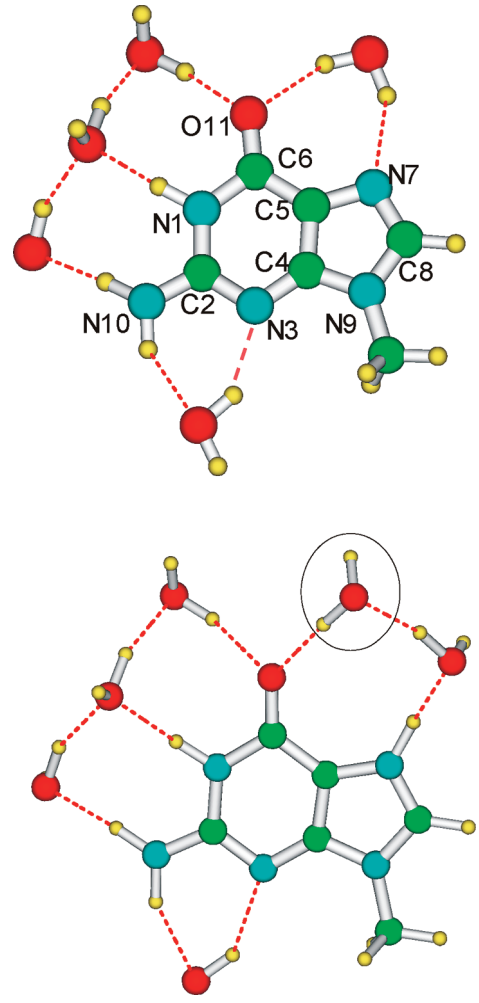

Figure 1. Schematic picture of neutral 9Me-G·5H_2O (top) and of protonated 9MeG-7H^+·6H_2O with an additional water molecule marked by circle (bottom).

equilibrium (EQ) solvation.[33,54] In the NEQ case, only solvent electrons equilibrate with the molecular excited state, whereas, in the EQ regime, also nuclear polarizations are equilibrated. For calculating absorption energies ν_A the NEQ limit is more suitable, while for emission ν_E the EQ regime must be used. All our calculations were performed by a development version of Gaussian03.[55]

3. Experimental Results

Stationary Spectra. Stationary absorption $A(\nu)$ and emission $E(\nu)$ spectra of GMP in water at pH 7−1 are displayed in Figure 2. Two absorption peaks at 36300 and 39600 cm^{-1} correspond to $S_0 \rightarrow L_a$ and $S_0 \rightarrow L_b$ transitions with oscillator strengths $f = 0.09$ and 0.17, respectively (the decomposed bands at pH 7 are shown by red lines). Note that $E(\nu)$ is calculated from the experimental fluorescence spectra $F(\lambda)$ (see Figure S1 in the Supporting Information) as $E(\nu) \approx \lambda^4 \cdot F(\lambda)$.[56] This way both absorption A and emission E are expressed in the same dimensional units of extinction (or cross-section) allowing for correct comparison between the two and with the transient ΔA absorption spectra.

At pH 7−4 the absorption spectra are nearly indistinguishable and correspond to neutral GMP. When pH is lowered further from

(47) Scalmani, G.; Frisch, M. J.; Mennucci, B.; Tomasi, J.; Cammi, R.; Barone, V. *J. Chem. Phys.* **2006**, *124*, 094107.
(48) Cossi, M.; Barone, V. *J. Chem. Phys.* **2001**, *115*, 4708–4717.
(49) Barone, V.; Improta, R.; Rega, N. *Acc. Chem. Res.* **2008**, *41*, 605–616.
(50) (a) Improta, R.; Barone, V.; Santoro, F. *Angew. Chem., Int. Ed.* **2007**, *46*, 405–408. (b) Improta, R.; Barone, V.; Santoro, F. *J. Phys. Chem. B* **2007**, *111*, 14080–14082.
(51) Improta, R.; Scalmani, G.; Frisch, M.; Barone, V. *J. Chem. Phys.* **2007**, *127*, 074504.
(52) Improta, R.; Barone, V.; Scalmani, G.; Frisch, M. J. *J. Chem. Phys.* **2006**, *125*, 054103.
(53) Kampf, G.; Kapinos, L. E.; Griesser, R.; Libbert, B.; Sigle, H. *J. Chem. Soc., Perkin Trans. 2* **2002**, 1320–1327.
(54) Cossi, M.; Barone, V. *J. Phys. Chem. A* **2000**, *104*, 10614–10622.
(55) Frisch, M. J.; et al. *Gaussian03 Development Version*, revision F.02; Gaussian Inc.: Wallingford, CT, 2007.
(56) Birks, J. B. *Photophysics of aromatic molecules*; Wiley-Interscience: 1970; Sections 3, 4, Figure 4.2

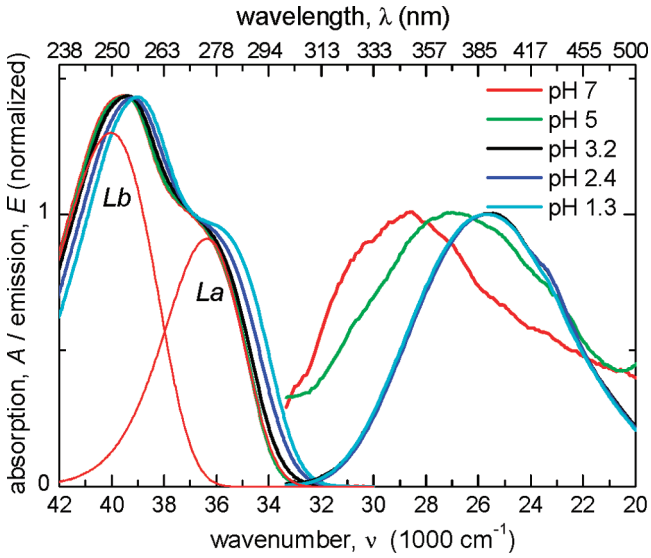

Figure 2. Absorption $A(\nu)$ and stimulated emission $E(\nu) = \lambda^4 F(\lambda)$ spectra from GMP in water at pH 7−1. $E(\nu)$ is calculated from the original fluorescence $F(\lambda)$ shown in Figure S1. Absorption peaks at 36 300 and 39 600 cm^{-1} correspond to $S_0 \rightarrow L_a$ and $S_0 \rightarrow L_b$ transitions (the decomposed bands at pH 7 are displayed in red) with oscillator strengths $f = 0.09$ and 0.17, respectively. The absorption red-shift at lower pH reflects ground-state protonation, with $pK_a = 2.5$ derived from the half-shift (occurring at pH 2.5). Emission spectra are extremely broad, especially at pH 7−5, indicating short-lived fluorescence. Absorption and emission spectra are normalized for better comparison.

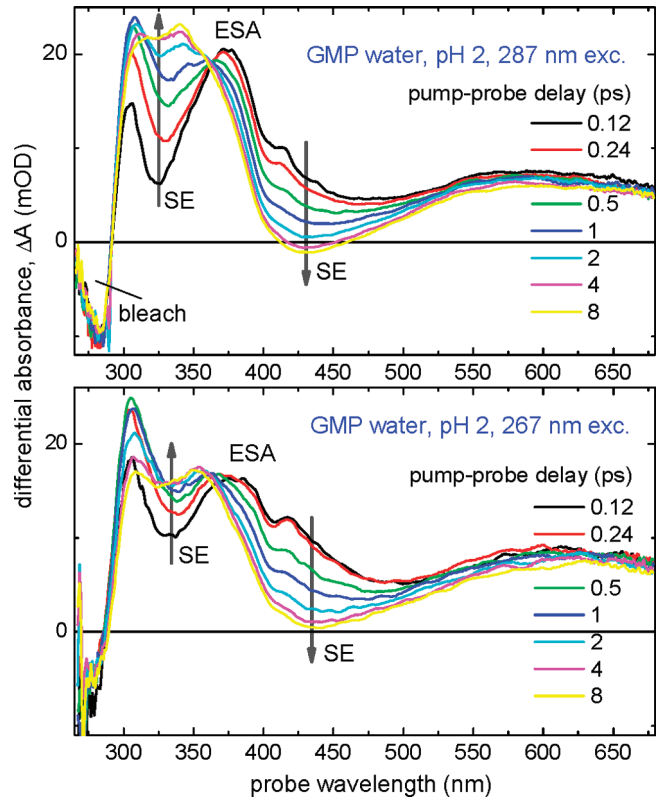

Figure 3. Transient absorption $\Delta A(\lambda,t)$ spectra from GMP in water at pH 2, measured with 287 nm (top) and 267 nm (bottom) excitation and parallel pump−probe polarization. Bleach and stimulated emission (*SE*) have negative amplitude, and excited-state absorption (ESA) is positive. The evolutions for the two excitation wavelengths are similar (see also Figures S6, S7), suggesting that $L_b \rightarrow L_a$ relaxation is ultrafast (unresolved, $\tau_{ba} \ll 100$ fs). A well-defined isosbestic point at 363 nm (with signal development shown by arrows) indicates a state-to-state relaxation. Two quasistationary states ($L_{a\,\mathrm{min}}^{\mathrm{planar}}$ and $L_{a\,\mathrm{min}}$) are recognized by their emission bands, one decaying at ∼320 nm and another developing at 425 nm (the bands are seen as spectral dips in a positive ESA background).

4 to 1.3, the absorption bands experience a red-shift (by 900 cm^{-1}) which was ascribed to ground-state protonation.[6] The corresponding $pK_a = 2.5$ (2.2 in ref 57) is derived from the half-shift (occurring at pH 2.5). The emission shift, occurring mainly in the pH range 7−4, is of a different nature and originates from an increasing fluorescence contribution of ground-state protonated species. Although this protonation is weak, less than 10^{-2} at pH 5 for example, and not visible in absorption, it is observable in emission due to the much longer fluorescence lifetime and higher emission intensity of $GMPH^+$. Note that if one assumes for the emission shift an excited-state protonation similar to that in the ground state, it would result in the excited-state $pK_a^* = 5$. The latter value is however inconsistent with transient absorption data, as discussed in the Supporting Information.

We observed an extremely wide emission band (7000 cm^{-1} at pH 7−5) and a large Stokes shift of 7000−10000 cm^{-1} when going from pH 7 to 1. These features together with a low emission quantum yield strongly suggest nonstationary short-lived fluorescence and substantial excited-state rearrangement of GMP.

Hot Absorption Spectra. When a photoexcited molecule experiences fast internal conversion, a hot ground state is formed which is observable in transient absorption as a *difference* between hot and cold ground-state spectra.[27] Thus hot transient spectra can be modeled by using temperature-dependent stationary spectra.[30] We measured the absorption spectra of neutral GMP at pH 7 in the temperature range 20−80 °C (Figure S2) and calculated the corresponding differential spectra which are used for comparison with transient absorption spectra.

Transient Measurements. As already mentioned GMP was excited at 267 or 287 nm. In aqueous solutions UV pumping generates solvated electrons which make an unwanted contribution to the signal. This contribution should be subtracted to result in correct GMP spectra.[9] A comparison between the solvent signal and that from GMP in solution and the procedure for subtracting solvent contributions, as well as comparison between 267 and 287 nm excitations, are discussed in the Supporting Information (Figures S3, S4 and S6, S7).

Transient Spectra at pH 2. It is convenient to start with pH 2 when most of the GMP molecules are ground-state protonated. The transient absorption $\Delta A(\lambda,t)$ spectra are displayed in Figure 3 for two excitation wavelengths, 287 nm (top) and 267 nm (bottom). Recall that bleach and stimulated emission (SE) enter $\Delta A(\lambda,t)$ with a negative amplitude, and excited-state absorption (ESA) is positive. According to Figure 2, pumping with 267 nm populates both L_a and L_b states, while with 287 nm only L_a is excited. Thus one may expect a different excited-state evolution for the two excitation wavelengths. However the difference between the two frames in Figure 3 is negligible (see also Figure S6). Only an isosbestic point at 363 nm, observed with 287 nm pumping, is slightly washed out upon excitation at 267 nm. Also, in the upper frame the signal $\Delta A(\lambda,t)$ at 425 nm becomes negative with time, while in the lower frame it does not. But in general the transient spectra behave quite similarly indicating that $L_b \rightarrow L_a$ relaxation is ultrafast and remains unresolved in our experiment. This gives an estimate $\tau_{ba} \ll 100$ fs for the $L_b \rightarrow L_a$ relaxation time.

One of the most significant features is the presence of an isosbestic point at 363 nm. To the left and right of this point the signals develop in opposite directions. Generally, such behavior strongly suggests a relaxation process between two quasistationary states. In the present case these states are recognized by SE bands seen as spectral holes on the positive ESA background. An SE band at 320 nm decays while another SE band concomitantly develops at 425 nm, in the region of stationary emission. The initial emission

(57) Börresen, H. C. *Acta Chem. Scand.* **1963**, *17*, 92.

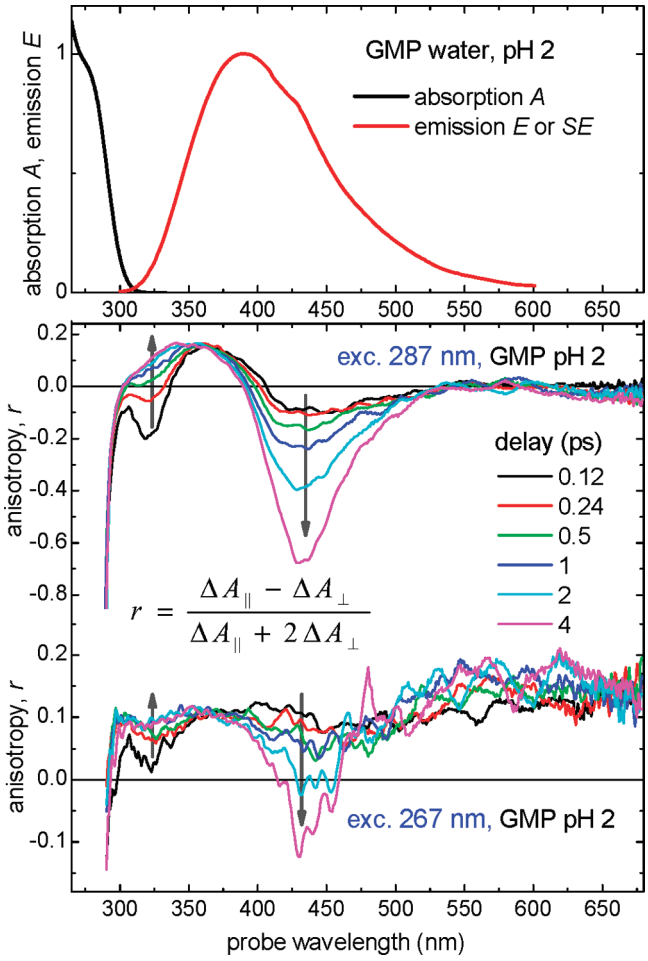

Figure 4. GMP in water, pH 2. Stationary spectra (top) and anisotropy transient spectra $r = (\Delta A_{\parallel} - \Delta A_{\perp})/(\Delta A_{\parallel} + 2\Delta A_{\perp})$ for excitation at 287 nm (middle) and 267 nm (bottom). A decaying band at ~320 nm and another one developing at 425 nm represent the same state-to-state relaxation as that in Figure 3. The evolution is again better defined at 287 nm excitation because 267 nm excites both L_a and L_b. The band $S_0 \rightarrow L_b$ is perpendicularly polarized to $S_0 \rightarrow L_a$ and to SE. Therefore excitation at 267 nm is less polarization-selective and results in weaker anisotropy signals.

at 320 nm (31600 cm^{-1}) is detuned from the $S_0 \rightarrow L_a$ absorption peak (at 35400 cm^{-1}) by 3800 cm^{-1}. This is close to the L_a absorption bandwidth which gives an estimate of the reorganization energy of the vibrational modes, suggesting that the SE band at 320 nm can be ascribed to the region of the potential energy surface (PES) reached just after relaxation of high-frequency modes.

The same relaxation process can also be seen in the transient anisotropy spectra $r = (\Delta A_{\parallel} - \Delta A_{\perp})/(\Delta A_{\parallel} + 2\Delta A_{\perp})$ presented in Figure 4. Here, the two emission bands are clearly recognized by their negative anisotropy. The sign can be understood recalling that ΔA = (ESA − SE) and that ESA is often only weakly anisotropic ($ESA_{\parallel} \approx ESA_{\perp}$) because its polarization is generally different from that of absorption and bleach. In our case, excitation at 287 nm selects molecules oriented such that their $S_0 \rightarrow L_a$ transition is parallel to the pump polarization. The polarization of SE, which monitors the same $L_a \rightarrow S_0$ transition, is of the same direction. Therefore there should be $SE_{\parallel} = 3 \cdot SE_{\perp}$ at early time (when neglecting rotational diffusion). Then the numerator in r becomes negative while the denominator is positive (provided ESA is stronger than SE as in the present case). And again as in ΔA spectra, the picture is much cleaner with 287 nm (Figure 4 top) than with 267 nm pumping. This is mainly because 267 nm excites both $S_0 \rightarrow L_a$ and $S_0 \rightarrow L_b$, the latter being perpendicularly polarized to $S_0 \rightarrow L_a$ and consequently to SE. Therefore excitation at 267 nm is less polarization-selective and results in weaker anisotropies (Figure 4, bottom).

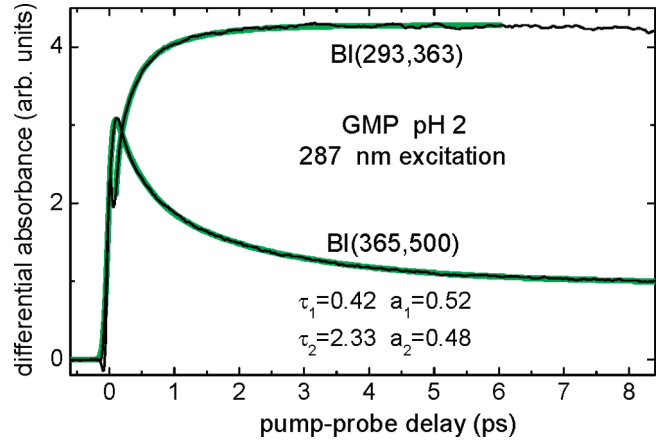

Figure 5. Band integrals for GMP in water, pH 2, upon 287 nm excitation. The behavior of the band integrals BI(293,363) and BI(365,500) left and right from the isosbestic point in Figure 3 (top) are given. A biexponential fit yields $\tau_1 = 0.42$ ps, $\tau_2 = 2.3$ ps with an average time $\langle \tau_{1,2} \rangle = 1.3$ ps.

Band Integral Analysis. A quantitative description of the photoinduced evolution can be obtained with band integral analysis.[27] The band integral $BI(\lambda_1,\lambda_2;t)$ is defined as

$$BI(\lambda_1, \lambda_2; t) = \int_{\lambda_1}^{\lambda_2} \Delta A(\lambda, t) \cdot (d\lambda/\lambda) \qquad (1)$$

where (λ_1,λ_2) is the wavelength range over which the integral is taken. The main advantage of the band integral over kinetics at selected wavelengths is that $BI(\lambda_1,\lambda_2)$ is insensitive to spectral diffusion over a broad spectral region. Then it reflects only the population dynamics and hence provides the corresponding time constants. In the present case there are two characteristic band integrals, BI(293,363) and BI(365,500), below and above the isosbestic point at 363 nm. These integrals are shown in Figure 5. Their behaviors are not fully consistent; BI(365,500) decays slower than its counterpart BI(293,363) increases. A possible reason may be a residual solvent contribution which is stronger in the UV or faster decay of 320 nm SE. A biexponential fit $a_1 \exp(-t/\tau_1) + a_2 \exp(-t/\tau_2)$ of the integral BI(365,500) results in $\tau_1 = 0.42$ and $\tau_2 = 2.33$ ps ($a_1 = 0.52$, $a_2 = 0.48$). The fit gives also the pump−probe cross-correlation $\tau_{cc} = 0.12-0.15$ ps (fwhm).

To complete the evaluation of the measurements at pH 2, Figure 6 shows the behavior of band integrals for anisotropy BI(325,375) (top) and for the transient signal BI(300,400) (measured at magic angle, bottom) on a long time scale. The fits give $\tau_R = 78$ ps for rotational diffusion and $\tau_3 = 167$ ps for the excited-state lifetime of $GMPH^+$.

Transient Spectra at pH 7. Figure 7 displays transient absorption spectra of neutral GMP at pH 7 (the spectra recorded for pH 3−5 can be found in the Supporting Information) measured with excitation at 287 nm (top) and 267 nm (bottom). The evolutions in the two frames are again quite similar confirming that the $L_b \rightarrow L_a$ relaxation is unresolved in our experiment. A quasiisosbestic point is now observed at $\lambda = 400$ nm. For $\lambda > 400$ nm the spectra decay monotonically, while for $\lambda < 400$ nm the signal first increases (between 0.12 and 0.24 ps) and then decays, as indicated by arrows. A complete spectral evolution is presented in Figure 8 where the two probe regions 270−690 nm and 340−1000 nm are combined together. The spectral behavior can be described with band integrals BI(400,900) and BI(270,400) shown in Figure 9. BI(400,900) decays biexponentially with $\tau_1 = 0.22$ ps, $\tau_2 = 0.87$ ps, whereas BI(270,400) can be fitted triexponentially with one growing, $\tau_1 = 0.25$ ps, and two decaying components, $\tau_2 = 1.0$ ps, $\tau_3 = 2.5$ ps. Note that the time constants τ_1, τ_2 of the two band integrals are in good agreement with previously measured fluorescence decay times 0.2 and 0.9 ps.[11,12]

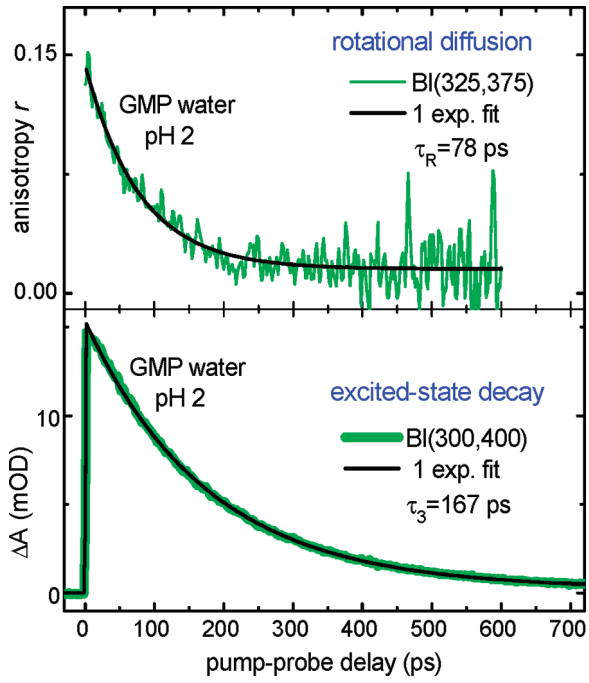

Figure 6. Band integrals for GMP in water at pH 2 with 287 nm excitation. Top: BI(325,375) for anisotropy decay gives $\tau_R = 78$ ps for rotational diffusion of $GMPH^+$ molecules. Bottom: The decay of BI(300,400) (measured at magic angle) results in $\tau_3 = 167$ ps for the excited-state lifetime of $GMPH^+$.

Next, BI(400,900) decays to zero, suggesting that GMP returns to the ground state; i.e., $\tau_2 = 0.9$ ps should represent internal conversion $L_a \rightarrow S_0$. Then the transient signal at $\lambda < 400$ nm, decaying with $\tau_3 = 2.5$ ps, has to be ascribed to vibrational cooling of hot ground-state molecules. The comparison between late (after 1 ps) transient spectra $\Delta A(\lambda,t)$ with hot stationary differential spectra $\Delta A(\lambda,\Delta T)$ (in the temperature range 293−353 K, see Figure S8) is in agreement with this picture. Further indications of fast internal conversion are also obtained upon analyzing the anisotropy behavior as presented in Figure 10. There, the evolution of anisotropy $r = (\Delta A_{\parallel} - \Delta A_{\perp})/(\Delta A_{\parallel} + 2\Delta A_{\perp})$ is shown for two spectral regions, at 300 nm (red edge of bleach) and ∼435 nm. With 287 nm excitation (blue) the anisotropy at 300 nm (top) changes from negative to positive values on a 1 ps scale. This agrees both with a time of internal conversion $\tau_2 = 0.9$ ps and with a positive anisotropy value of ground-state molecules. Remember that for hot ground-state transient anisotropy $r(t) = 0.4$ is expected when neglecting rotational diffusion. In fact this value is not reached because of a strong contribution from ESA peaked at 300 nm which is polarized differently from the bleach. This ESA band contributes to the signal even after 2 ps (see also Figure S8), when hot absorption starts to decay due to vibrational cooling. At 435 nm (bottom) the anisotropy is initially close to zero and decreases to negative values until $t =$ 0.25 ps, which may indicate development of a new emission band, similar to the case observed for pH 2 (see Figure 3). Also, the time scale is comparable to $\tau_1 = 0.2$ ps for the fastest component of the spectral evolution in Figure 7. As anticipated above, no such effects are observed with 267 nm pumping (red curve) because this excitation is less polarization-selective and results in anisotropy signals which are small even at early times.

Anisotropy measurements clarify the role of the L_b state in the photoinduced evolution. The transitions $S_0 \rightarrow L_a$ and $S_0 \rightarrow L_b$ are perpendicularly polarized; therefore when the two are excited with 267 nm, the resulting anisotropy $r(t)$ is weaker than that with 287 nm pumping which can populate only L_a. Figure 2 allows for a quantitative estimate of this effect. As seen from the decomposed absorption bands, excitation at 267 nm creates approximately equal populations of L_a and L_b, in which case the anisotropy is the direct sum of two contributions, $r = r_{La} + r_{Lb}$. With $r_{La}(0) = 0.4$ and $r_{Lb}(0) = -0.2$, this gives $r(0) = 0.2$. This explains the value $r(0) = 0.15$ measured in the fluorescence upconversion experiments.[11]

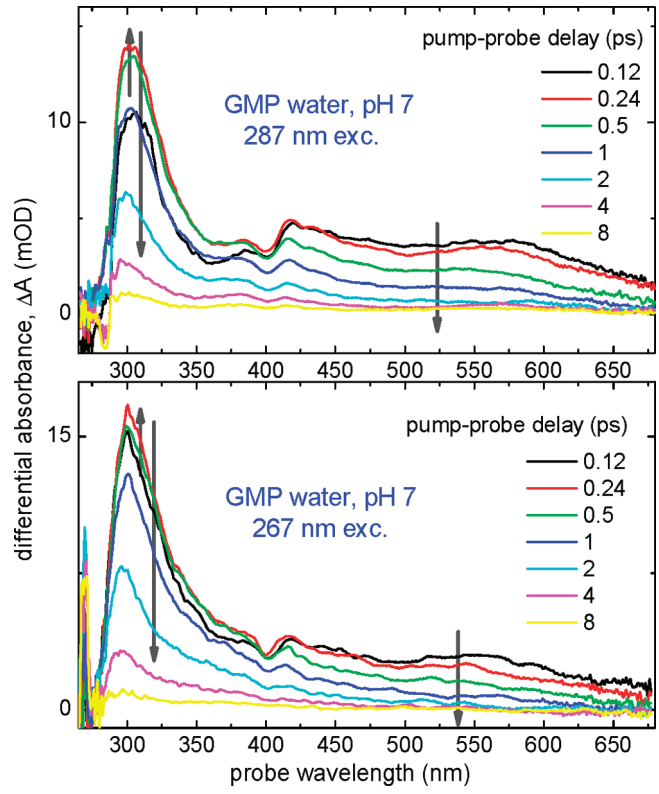

Figure 7. Transient absorption spectra $\Delta A(\lambda,t)$ from neutral GMP in water at pH 7 measured with 287 nm (top) and 267 nm excitation (bottom); pump−probe polarization is perpendicular. The evolutions in both frames are similar (see also Figures S6, S7), hence the $L_b \rightarrow L_a$ relaxation is unresolved ($\tau_{ba} \ll 100$ fs). A quasiisosbestic point is now observed at 400 nm. For $\lambda > 400$ nm the spectra decay monotonically, whereas for $\lambda <$ 400 nm the signal first increases (between 0.12 and 0.24 ps) and then decays, as indicated by arrows. The spectral evolution reflects the $L_{a\,\mathrm{min}}^{\mathrm{planar}} \rightarrow L_{a\,\mathrm{min}}$ relaxation followed by $L_{a\,\mathrm{min}} \rightarrow S_0$ internal conversion.

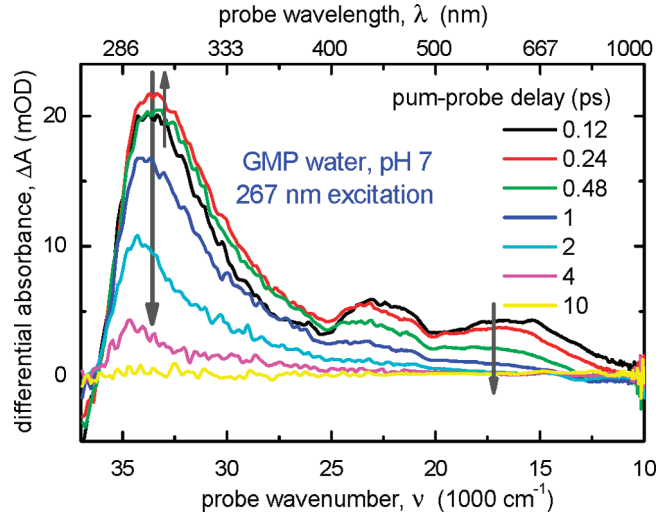

Figure 8. Transient spectra $\Delta A(\nu,t)$ of neutral GMP in water at pH 7 upon 267 nm excitation, obtained by combining two probe ranges 270−690 and 340−1000 nm. The evolution reflects the $L_{a\,\mathrm{min}}^{\mathrm{planar}} \rightarrow L_{a\,\mathrm{min}}$ relaxation followed by $L_{a\,\mathrm{min}} \rightarrow S_0$ internal conversion. The behavior is described with band integrals BI(400,900) and BI(270,400) shown in Figure 9. Note the ESA bands at 23000 cm^{-1} and 17000 cm^{-1} which shift by 1000 cm^{-1} to the blue in the course of decay.

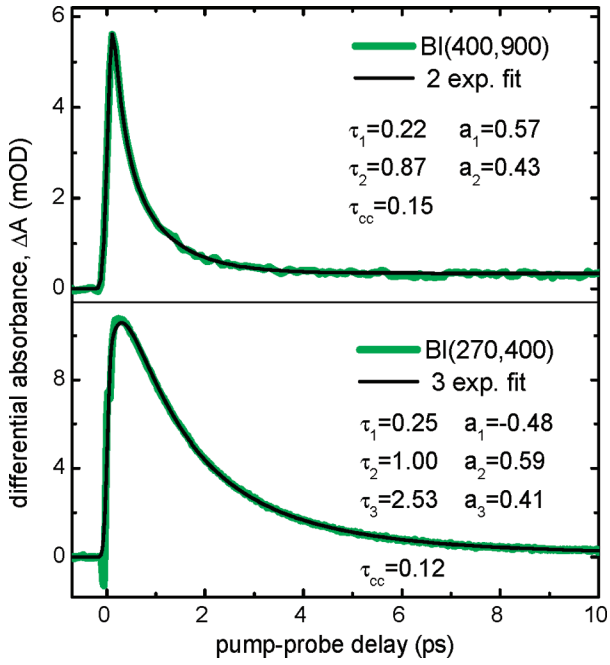

Figure 9. Band integrals for the spectral evolution in Figure 8. Top: BI(400,900) decays biexponentially with $\tau_1 = 0.22$, $\tau_2 = 0.87$ ps. Bottom: BI(270,400) is fitted with one growing, $\tau_1 = 0.25$ ps, and two decaying components, $\tau_2 = 1.0$, $\tau_3 = 2.5$ ps. The times τ_1 and τ_2 correspond to $L_a^{\text{planar}} \rightarrow L_{a\ \text{min}}$ and $L_{a\ \text{min}} \rightarrow S_0$ respectively, whereas τ_3 is ascribed to vibrational cooling of GMP molecules in the ground state S_0.

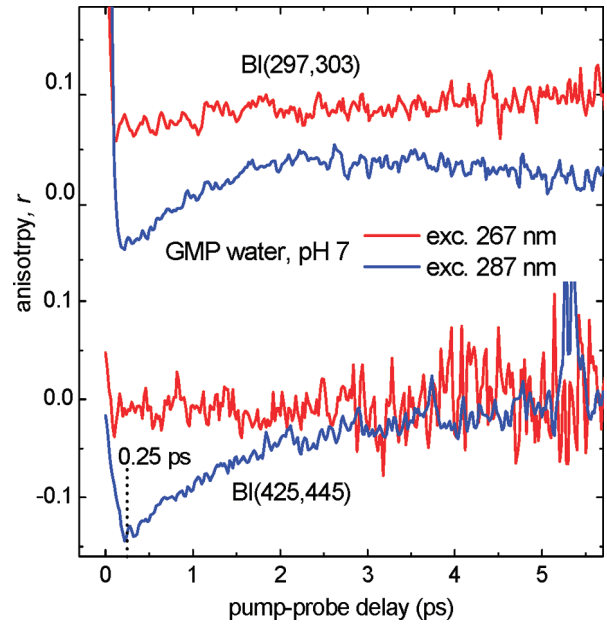

Figure 10. Transient anisotropy $r(t) = (\Delta A_{\parallel} - \Delta A_{\perp})/(\Delta A_{\parallel} + 2\Delta A_{\perp})$ upon excitation at 287 nm (blue) and 267 nm (red) for neutral GMP at pH 7. With 287 nm $r(t)$ at 300 nm (at the red edge of bleach, top) changes from a negative to positive value on a 1 ps scale. Such behavior is consistent both with $L_a \rightarrow S_0$ internal conversion and with a positive anisotropy of the ground-state molecules. Upon internal conversion, $r = 0.4$ is expected when neglecting rotational diffusion. This value is not reached because of a strong ESA band peaked at 300 nm, which contributes even after 2 ps. At 430 nm (bottom), r is initially small and increases rapidly (until 0.25 ps) in negative magnitude, indicating a new emission band similar to that for $GMPH^+$ (Figure 4). No such effects are observed with 267 nm pumping which excites two perpendicularly polarized $S_0 \rightarrow L_a$ and $S_0 \rightarrow L_b$ transitions; therefore the resulting anisotropy is small even at early time.

Summarizing the results on transient absorption measurements, we note several similarities between the excited-state evolution for protonated and neutral GMP. The most significant one is that the behavior recorded by pumping at 287 nm is similar to that obtained with 267 nm. Furthermore, although the situation is much clearer for $GMPH^+$, in both cases τ_1 reflects relaxation from one region of the L_a surface ($L_a^{\text{planar}}{}_{\text{min}}$, see Figure 11) to another region ($L_{a\ \text{min}}$) as evidenced in both transient absorption (Figures 3 and 7, 8) and anisotropy spectra (Figures 4 and 10). However, protonated and nonprotonated species have very different excited-state lifetimes, long for $GMPH^+$ and short for neutral GMP. These features will be discussed and explained below with the help of quantum-chemical calculations.

4. Computations

Absorption Spectra. Table 1 collects the vertical absorption energies ν_A of 9Me-G·$5H_20$ and of 9Me-G in water computed at both the LR-PCM and the SS-PCM levels. The lowest transition at 4.6 eV (37100 cm^{-1}) can be described as HOMO→LUMO; the excited state has π/π^* character and corresponds to $S_0 \rightarrow L_a$ (see Figure S8 for the frontier orbitals). Another strong band at 5.2 eV (41940 cm^{-1}) corresponds to the $S_0 \rightarrow L_b$ transition (HOMO→LUMO+1 excitation). The L_a peak and the gap between $S_0 \rightarrow L_a$ and $S_0 \rightarrow L_b$ are overestimated by only 0.15 eV (1200 cm^{-1}), and the corresponding oscillator strengths f are also correctly reproduced compared to the experiment (last column in Table 1).

Two dark electronic states are relatively close to L_b. One corresponds to $^1n\pi^*$ excitation with a significant contribution from the Lone Pair (LP) of the C6−O11 carbonyl group. It lies at 6 eV, i.e., 0.7 eV higher than L_b and 1.3 eV higher than the pump wavelength at 267 nm. Interestingly, in agreement with the CASPT2 results, TD-PBE0/6-31G(d) calculations indicate that the $^1n\pi^*$ ν_A is 5.48 eV in the gas phase, intermediate between that of L_a (5.12 eV) and L_b (5.55 eV). This result suggests that, as in uracil derivatives,[38−40] the $^1n\pi^*$ state is destabilized in water by the presence of hydrogen bonds involving the carbonyl groups. The $S_0 \rightarrow {}^1n\pi^*$ transition promotes an electron from the lone pair, which can potentially act as a hydrogen-bond acceptor, toward a more diffuse π^* molecular orbital, leading to weakening of the solute−solvent hydrogen bond. In fact the energy gap between $n\pi^*$ and the bright states is significantly smaller (by ∼0.2 eV, see Supporting Information) when only bulk effects are considered, confirming that the inclusion of the first solvation shell is important for a correct estimate of the relative stability of different electronic states.

Another dark singlet state (HOMO→LUMO+2 $\pi\sigma^*$)[20,36] lies at 5.54 eV. In agreement with CASPT2, it corresponds to a Rydberg state in the FC region. The LUMO+2 orbital is mainly localized at the N1, C2, and N3 atoms and has partial σ^* character with respect to the N1−H and N10−H bonds. In the gas phase $\nu_A = 4.88$ eV is predicted for $\pi\sigma^*$ at theTD-PBE0/6-31+G(d,p) level, similar to that for CASPT2 (4.90 eV). The TD-PBE0/6-31+G(d,p) calculations indicate that for the $\pi\sigma^*$ state in water the dipole moment $\mu(\pi\sigma^*) = 6.8$ D is similar to that of the ground state. In the presence of water molecules the σ^* orbital is indeed slightly confined, decreasing the corresponding dipole moment (see Supporting Information for details).

Absorption energies ν_A for the protonated species (9Me-GN7H^+) are collected in Table 1. In this case L_a and L_b correspond again to the lowest excited states. In agreement with the experiment, our calculations predict a red shift of the $S_0 \rightarrow L_a$ band and an increase of the L_a/L_b energy gap. The $n\pi^*$ state is somewhat stabilized under strongly acidic conditions, since its

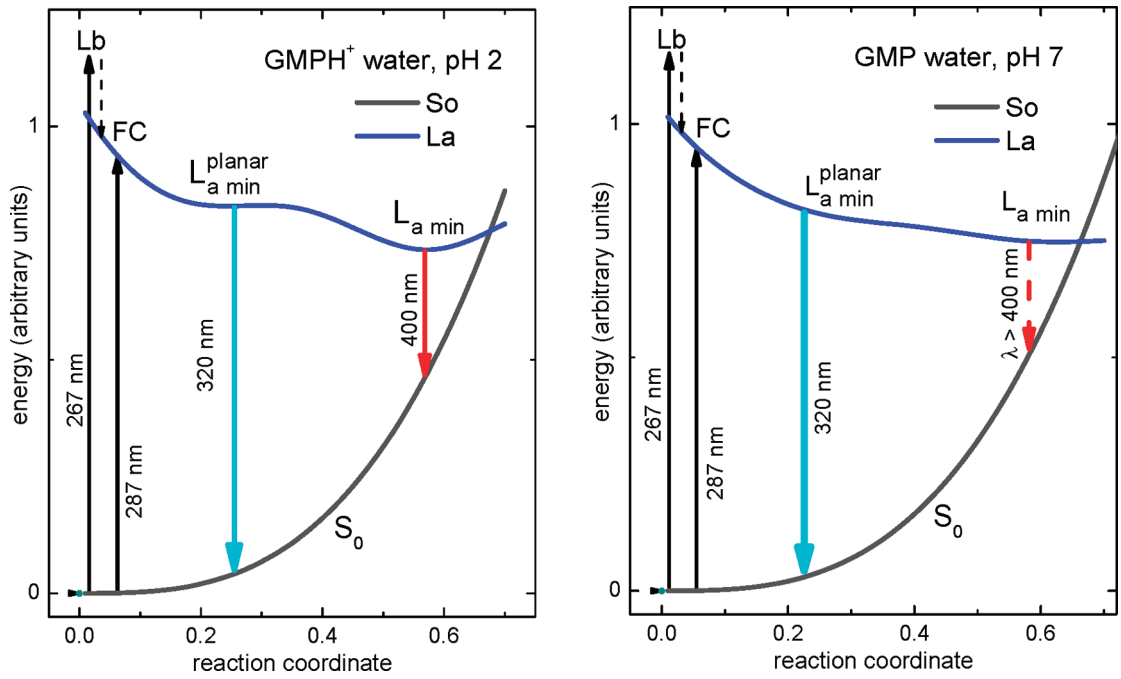

Figure 11. Scheme of the photoinduced evolution in protonated $GMPH^+$ (left) and neutral GMP (right). Pumping at 287 nm transfers the wave packet (WP) from S_0 to the FC region at the L_a state, while with 267 nm the WP is partly excited to L_b from where it converts ultrafast ($\tau_{ba} < 100$ fs) to the same FC region on L_a. Further evolutions for protonated and neutral species are qualitatively similar although proceed with different rates. For $GMPH^+$, the $L_a^{\text{planar}}{}_{\text{min}} \rightarrow L_{a\ \text{min}}$ transition occurs through a small barrier, biexponentially with $\tau_1 = 0.4$ ps and $\tau_2 = 2.3$ ps. Here the minimum $L_{a\ \text{min}}$is well-defined, with NH and CH groups displaced out of the molecular plane, with $L_a^{\text{planar}}{}_{\text{min}}$ and $L_{a\ \text{min}}$ emitting at 320 and 400 nm, respectively. Slower internal conversion $L_{a\ \text{min}} \rightarrow S_0$ for $GMPH^+$ occurs afterwards with $\tau_3 = 167$ ps. For neutral GMP (right) the evolution is much faster implying nearly barrierless processes. Here $\tau_1 = 0.22$ ps is ascribed to the $L_a^{\text{planar}}{}_{\text{min}} \rightarrow L_{a\ \text{min}}$ transition (although our calculations do not show a real minimum for neutral GMP, but only a monotonic decay, we use the same notation to stress the similarity with $GMPH^+$). Subsequent fast, $\tau_2 = 0.9$ ps, internal conversion (possibly solvent-controlled) results in a hot ground state which cools down with $\tau_3 = 2.5$ ps.

Table 1. Vertical Absorption Energies ν_A (in cm^{-1}) and Oscillator Strengths f for Neutral 9Me-G and Protonated 9Me-G-N7H$^+$ in Solution from the TD-PBE0 Method with Geometries Computed at the PCM/PBE0/6-31G(d) Level

	LR-PCM						SS-PCM				
	6-31G(d)		6-31+G(d,p)		6-311 +G(2d,2p)		6-31G(d)		best estimate[a]	experiment	
state	ν_A	f	ν_A	f	ν_A	f	ν_A	f	ν_A	ν_A	f
					9Me-G·5H$_2$O in Water						
L_a	39280	(0.14)	38310	(0.17)	37750	(0.16)	38960	(0.11)	37420	36320	(0.094)
L_b	43720	(0.33)	42180	(0.35)	41780	(0.34)	44520	(0.26)	42590	40030	(0.167)
nπ^*	46780	(0.00)	46860	(0.00)	46540	(0.00)	48390	(0.00)	48150		
$\pi\sigma^*$			44120	(0.00)	43630	(0.00)	44680[c]	(0.00)	44200		
					9Me-G-N7H$^+$·6H$_2$O in Water						
L_a	37180	(0.15)	36540	(0.17)	35730	(0.16)	38230	(0.12)	37020	35400	(0.09)
L_b	43470	(0.25)	42590	(0.29)	42260	(0.27)	44280	(0.17)	43070	39120	(0.16)
nπ^*	45810	(0.00)	45970	(0.00)	45560	(0.00)	45650	(0.00)	45490		
$\pi\sigma^*$			47830	(0.00)	47260	(0.00)					
					9Me-G-N7H$^+$·5H$_2$O in Water						
L_a	37670	(0.15)	36860	(0.17)	36380	(0.16)	38880	(0.12)	37590		
L_b	43070	(0.25)	42260	(0.29)	41940	(0.27)	44040	(0.20)	42910		
nπ^*	44280	(0.00)	44520	(0.00)	44200	(0.00)	44520	(0.00)	44440		
$\pi\sigma^*$			47430	(0.00)	46860	(0.00)	46050[c]	(0.00)	45490		

[a] Obtained by correcting ν_A from SS-PCM for the basis set effect estimated with LR-PCM. [b] Gas phase results for ME-G. TD/PBE0/6-31G(d): L_a = 41860 (0.15); L_b = 44760 (0.24); nπ^* > 44200 (0.00). TD-PBE0/6-31+G(d,p): $\pi\sigma^*$ 39360 (0.00). [c] SS-PCM/TD-PBE0/6-31+G(d,p) calculations.

energy gap with respect to the bright states decreases by 0.4 eV and becomes slightly more stable than the $\pi\sigma^*$ state.

Excited-State Geometry Optimizations and Relaxed Emission Spectra. As a further step we tried to optimize the equilibrium geometry of the lowest excited states, L_a and L_b which are accessible at our experimental conditions.

First we discuss the neutral species. Besides studying solvation by water and acetonitrile, we have performed optimizations of L_a in the gas phase, to compare the TD-PBE0 results with those from CASPT2. In the gas phase, our calculations predict no minima at the L_a surface and a barrierless path from the FC region to the proximity of L_a/S_0 CI, with the L_a/S_0 energy gap being less than 0.4 eV (3200 cm^{-1}). The CI is reached by pyramidalization at C2, with the ring adopting an envelope puckered structure, and with the out-of-plane motion of the amino substituent. This is the same picture as that provided by

Table 2. Vertical Absorption ν_A and Emission ν_E Energies (in cm^{-1}, the Energy of S_0 Is Taken as 0) and Oscillator Strength f of the $S_0 \rightarrow L_a$ Transition for 9Me-G and 9Me-G-H^+ in Water[a,b]

	S_0		Nonequilibrium solvation			Equilibrium solvation			Stokes shift
system	ν_A	f	ν_A^{neq}	f	ν_E^{neq}	ν_A	f	ν_E	$\nu_A-\nu_E$
9Me-G·5H_2O + PCM									
$L_{a\ min}^{planar}$	38960	(0.11)	37830	(0.11)	34840	36620	(0.11)	33310	5650
9Me-G-H^+·6H_2O + PCM									
$L_{a\ min}^{planar}$	38230	(0.12)	36130	(0.10)	33380	33230	(0.09)	29840	8390
$L_{a\ min}$	38230	(0.12)	34040	(0.10)	33070	29280	(0.09)	27580	10650
9Me-G-H^+·5H_2O + PCM									
$L_{a\ min}^{planar}$	38880	(0.12)	36780	(0.11)	34280		(0.10)	30000	8870
$L_{a\ min}$	38880	(0.12)	35490	(0.10)	30330	31860	(0.09)	25330	13550

[a] SS-PCM/TD-PBE0/6-31G(d) calculations on geometries computed at the PCM/PBE0/6-31G(d) level. [b] NEQ and EQ mean nonequilibrium and equilibrium solvation in the PCM framework, with the solvation shell corresponding to the excited-state minima $L_{a\ min}^{planar}$ and $L_{a\ min}$ (see Figure 11).

CASPT2 on guanine[21,22] supporting the reliability of our approach and putting the subsequent analysis on firmer ground. PCM/TD-PBE0 geometry optimizations for 9Me-G·5H_2O and for 9Me-G in water indicate that, after an initial very steep region, the L_a surface exhibits a flat plateau (with gradients < 0.001 au, hereafter L_a^{planar} with an almost planar purine ring), suggesting that emission should stem mainly from this region. Using the lowest gradient point in this region as reference pseudominimum $L_{a\ min}^{planar}$, the computed emission energy $\nu_E = 4.13$ eV (33310 cm^{-1}, see Table 2) is shifted by 5600 cm^{-1} from the absorption peak ν_A. This is consistent with the experimental Stokes shift of 7000 cm^{-1}. However, a barrierless path connects $L_{a\ min}^{planar}$ to the L_a/S_0 CI, which is reached by the out-of-plane motion of the amino substituent, while the ring adopts a puckered structure, as in the case of the gas phase. This result is in line with the short-lived fluorescence experimentally recorded and with the subpicosecond time constants we have reported in the present study. Furthermore, fluorescence will stem not only from this planar pseudominimum but also from other regions of the PES in the path leading to the L_a/S_0 CI. In these latter regions S_0 and L_a are closer together decreasing the emission energy, as shown by the red tail of the stationary emission spectrum shown in Figure 2.

Next, geometry optimization indicates that L_b should decay to L_a. Although only a quantum dynamical study can assess the rate of the $L_b \rightarrow L_a$ relaxation, our calculations show that the L_b surface in the region connecting the FC point and L_b/L_a crossing is strongly repulsive with a steep gradient, suggesting that the relaxation should be very fast. Extensive exploration of the L_b PES does not reveal any minima, in line with the absence of additional bands in the fluorescence spectra.

With respect to nπ^* and $\pi\sigma^*$ states we limit our analysis to the 9Me-G system in water. The nπ^* state exhibits a geometry of minimum energy similar to that obtained by Serrano-Andres et al.[21] in their gas phase calculations. However the minimum for the nπ^* state is less stable than that for L_a by 0.2 eV (PCM/TD-PBE0/6-31+G(d,p)). An even larger destabilization is expected for 9Me-G·5H_2O, due to the presence of solute−solvent hydrogen bonds. The $\pi\sigma^*$ minimum is also planar and corresponds to the third excited state, since it is considerably less stable than the L_a and L_b states.

Protonation noticeably affects the behavior of L_a. Excited state geometry optimizations of the L_a state in water (for 9Me-G7H^+·6H_2O, 9Me-G7H^+·5H_2O, and 9Me-G7H^+) lead to a pseudominimum region L_a^{planar} with extremely small gradients (<0.0004 au, i.e., smaller than the corresponding region in the neutral compound), where the purine ring keeps an almost planar structure as in the FC region. Actually, geometry optimizations converge to an equilibrium structure $L_{a\ min}^{planar}$. The emission energy of this region is red-shifted by 4500 cm^{-1} with respect to the absorption maximum (ν_E^{neq} in Table 2), in good agreement with the experimental SE band at 320 nm. However, vibrational analysis of $L_{a\ min}^{planar}$ shows imaginary vibrational frequencies, with the highest one corresponding to the out-of-plane motion of the hydrogens bonded to N7 and C8. This points to $L_{a\ min}^{planar}$ as a saddle point of the PES. Further optimizations lead to another stationary point $L_{a\ min}$ where all the frequencies are positive. In $L_{a\ min}$ the N7 and C8 hydrogens are out of the molecular plane (Figures S10, S11), with concomitant motion of water molecules in the first solvation shell. Interestingly, the emission energy ν_E from the pseudominimum $L_{a\ min}^{planar}$ is noticeably higher than that from $L_{a\ min}$ since the distorted planarity of $L_{a\ min}^{planar}$ leads to a significant destabilization of S_0. For example for 9Me-G7H^+·5H_2O, the emission energy ν_E from $L_{a\ min}^{planar}$ is blue-shifted by 4000−8000 cm^{-1} (depending if NEQ or EQ time regime is adopted for dynamical solvation) with respect to the stationary fluorescence from $L_{a\ min}$ (Table 2). This energy difference is similar to our experimental differences between the emission energies of the two quasi-stationary states responsible for the isosbestic behavior of L_a in $GMPH^+$. Furthermore, our finding that a real stationary point ($L_{a\ min}$) exists for L_a explains the much longer fluorescence lifetime measured for $GMPH^+$. Finally, the computed emission energy ν_E is significantly red-shifted from absorption ν_A, and the corresponding Stokes shift ($\nu_A-\nu_E$) is by 5000 cm^{-1} larger than that for neutral GMP, in close agreement with the experimental results.

For the protonated species no stationary point has been found on the L_b PES as well, and a fast decay to L_a is predicted.

5. Interpreting the Photoinduced Evolution of GMP

The information provided by our time-resolved experiments, when combined with the computational results, gives hints on the excited-state dynamics of GMP and $GMPH^+$.

As a first important conclusion, our study rules out any significant involvement of nπ^* and $\pi\sigma^*$ dark states in the GMP dynamics in water, both at neutral and at acidic pH. In fact, not only our computations predict that in water solution these states are significantly less stable than both L_a and L_b bright excited states, but also the experimental results indicate that the excited-state evolution involves only electronic states with a nonvanishing oscillator strength (vide infra)

Let us now discuss the possible involvement of the L_b excited state in the photoinduced dynamics of GMP. Also in this case, experiments and computations provide convergent results, showing that an ultrafast ($\tau_{ba} \ll 100$ fs) $L_b \rightarrow L_a$ decay occurs (see Figure 11), for both GMP and $GMPH^+$. Indeed, the spectra obtained at the 267 nm pump wavelength (when a significant part of the WP is excited to L_b) are quite similar to those obtained upon excitation at 287 nm, which brings the WP from S_0 almost exclusively to the L_a surface, as also indicated by the transient anisotropy experiments. All the complex spectral evolution revealed by the experiments has to be explained by the motion of the WP at the L_a surface only.

It is useful to start our analysis with the protonated $GMPH^+$ (Figure 11, at left), whose evolution is resolved better and can be used as a model for the interpretation of the GMP photodynamics.

Experiments indicate that the WP moves along L_a with some intrinsic time τ_i to a pseudostationary region, which, according to our computational results, can be identified as a planar region containing the $L_{a\,\mathrm{min}}^{\mathrm{planar}}$ pseudominimum. Experiments also indicate that this early motion FC$\rightarrow L_{a\,\mathrm{min}}^{\mathrm{planar}}$ is already complete before 100 fs. In fact, in the case of a slower decay time, the motion of WP would have to be visible in the time-resolved spectra as a dynamic shift of SE and ESA bands. SE would move to the red while ESA would shift to the blue reflecting stabilization of the WP on L_a. No such effects are present in the transient spectra after $t = 0.12$ ps (Figure 3), indicating that $\tau_i < 100$ fs.

After this time the spectral evolution is well-resolved and characterized by isosbestic behavior indicating a state-to-state relaxation process, which proceeds biexponentially with $\tau_1 = 0.4$ ps, $\tau_2 = 2.3$ ps. However we underline that these two times describe a single process since the characteristic isosbestic point persists for a longer period of time, until $t = 8$ ps when the process is complete (Figure 3). The relaxation involves two regions of the PES from which emission at 320 and 400 nm, respectively, occurs with similar intensity, confirming that a single electronic state is involved. Our computations indicate that a minimum on L_a ($L_{a\,\mathrm{min}}$) is present, emitting at ~400 nm, where the purine ring is not planar anymore, since the NH and CH groups are displaced out of the molecular plane (Supporting Information, Figure S12). Therefore we can assign τ_1 and τ_2 to the $L_{a\,\mathrm{min}}^{\mathrm{planar}} \rightarrow L_{a\,\mathrm{min}}$ relaxation. Although some alternative explanations could in principle be possible, the isosbestic behavior strongly suggests the existence of a barrier between these two regions of the PES. Actually, previous quantum-dynamical studies on retinal photodynamics show that, in the presence of a wide plateau on the excited-state PES, as we find for both GMP and $GMPH^+$, already a tiny barrier (<500 cm^{-1}) is sufficient to induce a biexponential decay.[58] It is clear that excited-state computations in solution on sizable molecules are not expected to have this degree of accuracy, especially if a substantial rearrangement of the solvation shell is associated with the WP motion as in the $L_{a\,\mathrm{min}}^{\mathrm{planar}} \rightarrow L_{a\,\mathrm{min}}$ transition. This process should also affect the outer solvation shells, which are not included in our model.

Finally, on a significantly longer time scale (in line with the substantial fluorescence quantum yield of L_a in $GMPH^+$) the WP leaves $L_{a\,\mathrm{min}}$, through internal conversion to S_0, with $\tau_3 = 167$ ps.

For neutral GMP the photoinduced evolution is much faster, and the spectral behavior is not as resolved as that for $GMPH^+$. For example, the quasi-isosbestic point is less clear, and the emission bands associated to different regions of the PES are not easily recognizable. Nonetheless, experiments and computations suggest an interpretation similar to that proposed for $GMPH^+$ (Figure 11 at right). As discussed above, the absence of any spectral shift in the ESA indicates that the motion away from the FC region is unresolved in our experiments; i.e., it occurs in less than 100 fs. The shortest time $\tau_1 = 0.2$ ps is thus due to the interplay between two different region of the PES, whose existence is also revealed by distinctive features of the steady state emission spectra (red curve in Figure 2.) One is associated with the peak of the fluorescence spectra at 340 nm, and the other to the extended red tail of the spectrum. Computations indicate that the former corresponds to the planar plateau of L_a containing the $L_{a\,\mathrm{min}}^{\mathrm{planar}}$ pseudominimum, while the latter is associated to the nonplanar part of the L_a PES, leading to the conical intersection with the ground state. The presence of the quasi-isosbestic point in our spectra suggests an energy barrier between $L_{a\,\mathrm{min}}^{\mathrm{planar}}$ and the nonplanar part of the PES. In any case, the very short time component of this process indicates that such a barrier would be very small, $\sim kT$.

The second time $\tau_2 = 0.9$ ps corresponds to the internal conversion from the nonplanar region of L_a to the ground state. At this poing we cannot unambiguously assess if a small energy barrier[16] is associated to this latter transition. Figure 8 shows that the ESA bands at 23000 cm^{-1} and 17000 cm^{-1} shift by 1000 cm^{-1} to the blue (as expected) in the course of decay. The time $\tau_2 = 0.9$ ps for the shift and decay, coincident with the longest solvent relaxation time in water (1.0 ps),[22] may indicate that the internal conversion is controlled by the solvent.

Finally, the slowest time component ($\tau_3 = 2.5$ ps) is ascribed to ground-state vibrational cooling.

6. Concluding Remarks

We have reported the results of a thorough study of the excited states dynamics of guanosine-monophosphate (GMP) in water. The behavior following excitation at 265 and 287 nm has been investigated by broad-band transient absorption spectroscopy in the range 250−1000 nm. The effect of the pH on the excited-state decay has been assessed by performing the same analysis in the pH range 2−7, confirming that in strongly acidic conditions the guanine ring is protonated. The results of the excited-state experiments have been interpreted by the help of quantum-mechanical calculations in aqueous solution, including also the water molecules of the first solvation shell in the model system studied. The computed absorption and emission spectra are in good agreement with their experimental counterparts for both the neutral and the protonated GMP, supporting the reliability of our computational approach.

Our study unveils the complexity of the processes underlying the GMP excited-state dynamics, characterized by strong multiexponential decay. On the other hand, our data indicate for the first time that only one excited state, namely L_a, the lowest energy adiabatic state, is significantly involved in the photodynamics following excitation in the near-UV. In contrast, other excited states such as $n\pi^*$ and $\pi\sigma^*$ dark states, whose participation has been often invoked for interpreting time-resolved experiments in the gas phase, do not play any significant role in the dynamics in water. Furthermore, the bright L_b state, which is also excited by the pump at 267 nm, decays to L_a within 100 fs and thus is not involved in the dynamics at longer times.

Actually, the photodynamics of GMP and $GMPH^+$ is controlled by the interplay between planar and nonplanar regions of the L_a PES. In the first part of the dynamics the purine ring keeps a planar geometry, as in the FC region, staying for a period of time in a flat plateau region. Later, the system evolves toward a nonplanar geometry, leading to a Conical Intersection with S_0 in the case of GMP, and to a nonplanar minimum in the case of $GMPH^+$. As discussed above, in the presence of a shallow PES a very small barrier can give rise to biexponential decay. Interestingly, a biexponential decay of the bright excited state is found also in other nucleobases, like thymine and its derivatives.[39,40] In these systems, a planar pseudominimum is predicted by computations also, followed by "nonplanar" decay toward the absolute minimum and/or a conical intersection with the ground state.[39,40] It is thus likely that also in these systems,

(58) Olivucci, M.; Lami, A.; Santoro, F. *Angew. Chem., Int. Ed.* **2005**, *117*, 5248–5251.

a biexponential decay, often considered as a signature for the involvement of different excited states, is due to the peculiar shape of the bright excited-state PES. In this regard, recent studies have shown that multiexponential decay can also be explained by the existence of multiple reaction paths[59] (not necessarily passing through excited-state minima) or by the presence of large conical intersection seams[60] with the ground state.

It is not possible, at the moment, to ascertain if the present results can give hints also on the excited-state decay in the gas phase. Actually, solvent significantly affects the GMP photodynamics. The energy ordering of the different excited states is very different with respect to that found in the gas phase, and solvent likely affects also the shape of the L_a PES. For example, it is noteworthy that the ground-state conversion in neutral GMP ($\tau_2 = 0.9$ ps) is probably controlled by the solvent. Actually, the out-of-plane motion of the amino substituent is expected to lead to a significant rearrangement of the GMP solvation shells, since two water molecules are hydrogen bonded to the $-NH_2$ group in aqueous solution, in which both participate in the water hydrogen bonding network. It is clear that this could remarkably affect the dynamical behavior of guanine, in line with a slower excited-state decay with respect to the gas phase.

The above considerations clearly show that the excited-state dynamics of sizable molecules in solution is governed by the interplay of many different physical effects, making their interpretation on the basis of oversimplified "excitation−internal conversion" models and simple kinetic schemes difficult. In this respect, appropriately tailored quantum-dynamical studies could be very useful, allowing for a direct comparison with time-resolved experiments. However, the present study shows that the integration of advanced experimental techniques and computational methods (allowing an accurate treatment of still larger systems under conditions increasingly more similar to those of the experiments) allow us to gain fundamental insight into the excited-state dynamics of the building blocks of life.

Acknowledgment. We thank the Deutsche Forschungsgemeinschaft for support and Niko Ernsting for stimulating this project, experimental contributions, and discussions. R.I. thanks Prof. Barone and Dr. Fabrizio Santoro for useful discussions.

Supporting Information Available: Additional results include temperature-dependent and pH-dependent spectra, comparison of the transient spectra and kinetics measured with 287 and 267 nm pumping, and computational details concerning the treatment of the $^1\pi\sigma^*$ state in solution, schematic drawing of the Guanine frontier orbitals, figures reporting the main geometrical parameters of the L_a minima, additional tables of the computed spectra in solution, Cartesian coordinates of the computed stationary points, and complete authors' list of ref 55. This material is available free of charge via the Internet at http://pubs.acs.org.

JA810092K

(59) Improta, R.; Santoro, F. *J. Chem. Theory Comput.* **2005**, *1*, 215–229.
(60) Hunt, P. A.; Robb, M. A. *J. Am. Chem. Soc.* **2005**, *127*, 5720–5726.